

Valorization of *Crataegus azarolus* stones for the removal of textile anionic dye by central composite rotatable design using cubic model: optimization, isotherm, and kinetic studies

Noreddine Boudechiche¹ · Hynda Yazid¹ · Mohamed Trari² · Zahra Sadaoui¹

Received: 31 January 2017 / Accepted: 21 June 2017 / Published online: 5 July 2017
© Springer-Verlag GmbH Germany 2017

Abstract In this study, the central composite rotatable design (CCRD) was used in the optimization of the operating parameters for the removal of the direct blue 86 (DB86), an anionic dye, because of its hazardous impact on human health and aquatic environment. In addition, DB86 is a recalcitrant and non-biodegradable dye whose presence considerably inhibits photosynthesis. Its removal in aqueous medium was achieved by biosorption onto the novel biosorbent *Crataegus azarolus* stones (CAS). The parameters like the solution pH, biosorbent dose, initial DB86 concentration, and temperature were studied in the ranges 2–6, 0.8–4 g L⁻¹, 20–100 mg L⁻¹, and 10–50 °C, respectively. The significance of the experimental parameters and their interactions was investigated by the Student's *t* test and *p* values with 5% error limits using JMP 11.0.0 software. The regression analysis of the experimental data obtained from 31 batch runs provides a cubic model. The optimum conditions obtained for the maximum DB86 elimination from the synthetic solution were found to be pH 2, biosorbent dose of 4 g L⁻¹, initial DB86 concentration of 20 mg L⁻¹, and temperature of 10 °C, leading to a theoretical maximum removal of 123%. The experimental data were analyzed by the Langmuir, Freundlich, and Temkin equilibrium models. The Langmuir isotherm gave the best fit with a maximum biosorption capacity of 24.02 mg g⁻¹. The results of the kinetic study revealed that the biosorption kinetic of DB86

follows a pseudo-second-order model. All results confirmed that CAS are an efficient, economic, and ecological alternative for the treatment of industrial wastewaters loaded with anionic dyes.

Keywords Direct blue 86 anionic dye · *Crataegus azarolus* stones · Central composite rotatable design · Biosorption isotherms · Kinetic modeling

Introduction

Dyes are classified as non-ionic (disperse), anionic (direct, acid, and reactive), and cationic (basic) compounds (Kuppusamy et al. 2016). Chemically, the anionic dyes consist of anthraquinone acid, triphenylmethane, xetonimina, azin, xanthenes, and nitro compounds. These dyes are used in the fiber industries like wool, silk, nylon, and acrylic-modified fibers (Silva et al. 2012). Currently, there are more than 100,000 types of dyes commercially available in the textile industry (Abbas and Trari 2015; Boudechiche et al. 2016). About 130 t of dyes is ejected daily into the aquatic environment without any control, and the cost to remove dyes remains high (Kuppusamy et al. 2016). In this respect, many methods are employed to reach the regulatory standards for treating wastewaters such as biological treatment (Aytar et al. 2013; Mozia et al. 2016), coagulation and flocculation (Verma et al. 2012), precipitation (Šimek et al. 2016), solvent extraction (El-Ashtoukhy and Fouad 2015), adsorption onto activated carbon (Noorimotlagh et al. 2014), membrane filtration (Mozia et al. 2016), electrochemical treatment (Mook et al. 2017), sonochemical degradation (Ferkous et al. 2015), photocatalysis using nanoparticles and nanocomposites (Yola et al. 2014a; Gupta et al. 2015), and advanced oxidation process (AOP) (Aytar et al. 2013; Mozia et al. 2016).

Responsible editor: Angeles Blanco

✉ Noreddine Boudechiche
N.BOUDECHICHE@univ-dbk.m.dz

¹ Laboratory of Engineering Reaction, Faculty of Mechanical and Processes Engineering, USTHB, BP 32, Algiers, Algeria

² Laboratory of Storage and Valorization of Renewable Energies, Faculty of Chemistry, USTHB, BP 32, Algiers, Algeria

However, these techniques have some disadvantages like the high energy and product consumption, incomplete removal, and generation of toxic sludge and other waste products, which require further treatments (de Luna et al. 2013). Among the physicochemical methods, biosorption using natural materials remains attractive, because of its efficiency, low cost, simplicity (Yola et al. 2014b; Gupta et al. 2016), elimination of various pollutants, abundance in nature, and biodegradability (Silva et al. 2012; Oladipo et al. 2014). Many biosorbents and waste materials have been tested for the removal of hazardous dyes and heavy metals in aqueous media such as the leaves of *Posidonia oceanica* (El Khames et al. 2014), *Inula viscosa* (Kebir et al. 2015), *Citrus limetta* peel (Pathak and Mandavgane 2015), rice husk (Li et al. 2016), *Luffa cylindrica* (Boudechiche et al. 2016; Kesraoui et al. 2016), jujube shell (El Messaoudi et al. 2016), olive stones (Albadarin and Mangwandi 2015), and de-oiled karanja seed cake (Varala et al. 2016). Agricultural wastes consist of cellulose, hemicelluloses, and lignin, which make them effective biosorbents due to their different functional groups. In this context, the new genus *Crataegus*, belonging to the Rosaceae family, is one of the most important genera. *Crataegus* species are available in many countries especially in North Africa (Khiari et al. 2014). The *Crataegus azarolus* (CA) wild fruits are known as pome, which are local and abundant in Algeria. They are used as a medicinal herb in the pharmaceutical and food industries; the seeds and their bony endocarps are termed stones which can degrade in 5–10 years. So, the objective of this study concerns the valorization of *C. azarolus* stones (CAS) as a new biosorbent for water depollution. To our knowledge, there are no published reports on CAS for dye removal and CAS can be attractive to replace high-cost biosorbents.

The response surface methodology (RSM) is a combination of statistical and mathematical methods used to develop, improve, and optimize the processes and to evaluate the relative significance of various process parameters in the presence of complex interactions (Jain et al. 2011). RSM was used in chemistry, physics, biology, and water treatment. Dye biosorption using RSM permits us to fit the mathematical models to the experimental data using a minimal number of experiments to get the optimal parameters; this was undertaken with the goal of realizing the water treatment in less time and at low cost (Jain et al. 2011; Gorgulu and Celik 2013; Akar et al. 2014; Asfaram et al. 2016; Salehi et al. 2016; Varala et al. 2016). RSM is a powerful tool for the prediction of engineering processes and is applied in many common designs such as Box–Behnken, Doehlert, and central composite rotatable designs (CCRD). The CCRD method includes factorial points from a full factorial (2^k), axial points ($2k$), and center points (cp). The number of experiments is estimated by $N = 2^k + 2k + cp$, where k is the factor number and cp is the replicate number of central points (Jain et al. 2011; Ahmadi et al. 2012). Central composite design (CCD) is a

RSM design which proposes a series of experiments with the least number of tests (Mazaheri et al. 2015). However, in some cases, the first-order and quadratic models developed by RSM do not fit well the experimental data (Afshar et al. 2015). Despite the fact that the cubic regression functions (X_i^3) have rarely been applied to the experimental data, when the responding variable is sensitive to changes of variables, the interaction between the parameters is deemed to be of vital importance; a third-order model provides a broader understanding of the process' nature (Bazrafshan et al. 2015). Podstawczyk et al. (2015) studied the effect of operating parameters for Cu^{2+} removal in the concentration range 20–200 mg L^{-1} , biosorbent dose 1–10 g L^{-1} , and pH 2–5 which were modeled by the comparison of three designs: CCD, Box–Behnken design (BBD), and full factorial design (FFD). The second-order polynomial equation extended with additional cubic effects was used as an objective function. The authors showed that CCD turned out to be the best design among the experiments for modeling the effect of the process conditions in terms of correlation coefficient ($R^2 = 0.99$) and ANOVA (Fisher value of 276 with p value lower than 0). The obtained model was further used to get the optimal conditions, which maximize the biosorption yield expressed by the metal removal.

The main goals of the present work include the following steps: (i) preparation and characterization (MEB/EDS, FTIR, and pH_{PZC}) of *C. azarolus* stones (CAS) as a novel biosorbent for DB86 anionic dye removal, used in Algeria for dyeing in the textile and clothing industries; (ii) application of CCRD based on a cubic polynomial module for the optimization of the operating parameters that affect the DB86 removal such as the solution pH, biosorbent dose, initial DB86 concentration, and temperature; and (iii) evaluation of appropriate biosorption isotherms and kinetic models for describing the DB86 biosorption.

Materials and method

Preparation of *C. azarolus* powder

Stones of *C. azarolus* were collected from the region of Mila (east Algeria), repeatedly washed with hot distilled water to eliminate the impurities, and dried at 80 °C for 24 h. Afterward, CAS samples were crushed and ground by a stainless steel grinder to get sizes smaller than 315 μm by standard sieves. The resultant powder was stored in airtight glass bottles for further experiments (Fig. 1).

Preparation of aqueous DB86 solution

DB86 was obtained from TEXALG textile unit of Boufarik (Algiers area). The stock solution was prepared by dissolving 1 g of DB86 in 1 L of distilled water. The solutions at different concentrations (20–100 mg L^{-1}) were prepared by dilution.

Fig. 1 Images of the *Crataegus azarolus*. **a** Fruits. **b** Stone. **c** Powder (<315 μm)



DB86 is anionic in nature, and its maximum absorption wavelength (λ_{max}) is 620 nm; other characteristics are reported in Table 1.

Determination of zero-charge pH

The zero-charge pH (pH_{PZC}) of CAS was determined by the technique described elsewhere (Boudechiche et al. 2016). Fifty milliliters of KNO_3 solutions ($\times 10^{-2}$ M) was transferred into 100-mL beakers. The initial pH ($pH_{initial}$) of the solutions was adjusted in regions 2–12 by addition of NaOH or HCl. Then, 0.5 g of CAS was added to the beakers, which was magnetically stirred for 48 h to reach the equilibrium, and the pH_{final} was measured. The difference ($pH_{initial} - pH_{final}$) was plotted against $pH_{initial}$. The intersection point of the resulting curve with the abscissa axis, for which $\Delta pH = 0$, gives $pH_{PZC} = 5.06$ (Fig. 2).

Scanning electron microscopy–energy-dispersive X-ray spectroscopy

The surface morphology of CAS was analyzed by scanning electron microscopy (SEM), JEOL-JSM 6360, combined with the energy-dispersive X-ray spectroscopy (EDS) to determine the chemical composition.

FTIR analysis

The FTIR spectroscopy was used to detect the surface functional groups of the biosorbent. The spectrum was recorded in the range 4000–650 cm^{-1} using a Fourier transform infrared spectrometer (Thermo Scientific™ OMNIC™ series software).

Central composite rotatable design and batch experimental program

CCRD is well-suited for fitting the polynomial surface and works well for the process optimization; it was used for the experimental design to obtain the optimal biosorption conditions (Sun et al. 2014). To evaluate the influence of the variables on the response functions and to establish the optimal

conditions of dye removal, we have used CCRD for the experiment design. In this study, 31 runs for the four-parameter experimental design were required to calculate the response function and to assess the design performance through the analysis of the experiment data. Moreover, the optimization process includes the evaluation of coefficients, thus predicting and verifying the response of the adjusted model. Therefore, four process variables, namely, pH of the solution (X_1), biosorbent dose (X_2), initial DB86 concentration (X_3), and temperature (X_4), were chosen, each at five levels ($-\alpha, -1, 0, +1, +\alpha$) (Table 2). CCRD for the four parameters consists of 16 factorial points, 6 axial points, and 7 replicates at the center point, with a total number of 31 experiments designed by JMP 11.0.0 (SAS Institute) software (Demim et al. 2013). The coded values (X_i) of the process variables were obtained from Eq. (1) (Kousha et al. 2015):

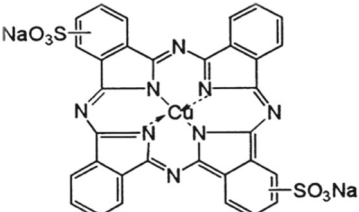
$$X_i = \frac{X_{i\ real} - X_{0\ real}}{\Delta X} \tag{1}$$

where X_i is the dimensionless coded value of the independent variable i , $X_{i\ real}$ is the real value, $X_{0\ real}$ is the value of X_i at the center point, and ΔX is the step change value. The empirical third-order polynomial model defines the behavior of the system using RSM, a cubic polynomial equation (Soo et al. 2004; Xie et al. 2011). Equation (2) was developed for the response prediction as a function of the main factors and their interactions. CCRD consists of a group of empirical techniques for establishing the relationship between a cluster of independent variables and the measured responses for the optimization of independent variables:

$$Y (\%) = a_0 + \sum_{i=1}^4 a_i X_i + \sum_{i=1}^4 a_{ii} X_{ii}^2 + \sum_{i=1}^4 a_{iii} X_{iii}^3 + \sum_{i=1}^3 \sum_{j=i+1}^4 a_{ij} X_i X_j + \sum_{i=1}^2 \sum_{j=i+1}^3 \sum_{k=j+1}^4 a_{ijk} X_i X_j X_k + \sum_{i=1}^1 \sum_{j=i+1}^2 \sum_{k=j+1}^3 \sum_{l=k+1}^4 a_{ijkl} X_i X_j X_k X_l \tag{2}$$

where Y is the predicted response (% removal), a_0 is a constant, a_i is the linear term coefficients, a_{ii} is the quadratic term

Table 1 Molecular properties of direct blue 86

Molecular formula	C ₃₂ H ₁₄ Cu ₈ Na ₂ O ₆ S ₂
Molecular weight	780.16 g mol ⁻¹
Colour index	74180
Synonyms	C.I. Direct Blue 86 (6CI) ; Cuprate(2-), [29H, 31H - phthalocyanine-C,C-disulfonato(4-)-N29, N30, N31, N32]-, disodium ; Turquoise Blue GL200
Chemical structure of DB86.	

coefficients, a_{iii} is the cubic term coefficients, and a_{ij} , a_{ijk} , and a_{ijkl} are the cross-product term coefficients. X_i , X_j , X_k , and X_l represent the independent variables in the form of coded values. The coded and real values of the independent variables are listed in Tables 2 and 3. Using the developed model, the predicted responses are compared with the observed values.

The residual DB86 concentrations were analyzed using UV/Vis spectrophotometer (Optizen 2120UV). The kinetic and equilibrium studies were investigated by using the optimum biosorption conditions. The amount of biosorbed DB86 q_t (mg g⁻¹) and DB86 removal (%) were calculated from Eqs. (3) and (4):

$$q_t = \frac{(C_0 - C_t)}{m} V \quad (3)$$

$$\% \text{Removal} = \frac{(C_0 - C_t)}{C_0} 100 \quad (4)$$

where C_0 is the initial DB86 concentration (mg L⁻¹), C_t is the DB86 concentration at time t (mg L⁻¹), m is the biosorbent mass (g), and V is the volume of the solution (L).

Results and discussion

Characterization of the biosorbent

FTIR analysis of the biosorbent

The FTIR spectrum of CAS is plotted in the range 4000–650 cm⁻¹ to get information on the functional groups on the biosorbent surface. The spectrum (Fig. 3) shows a strong peak at 3350 cm⁻¹ assigned to the O–H stretching vibration of OH groups involved in hydrogen bonds. The bands centered at 2929 and 2855 cm⁻¹ are assigned to C–H bond of alkyl

groups. The peaks at 1733, 1644, and 1234 cm⁻¹ are attributed to the stretching of C=O and COO⁻ functions (Vijayaraghavan et al. 2008) while the large band at 1644 cm⁻¹ is due to OH bending vibrations. The peak at 1504 cm⁻¹ is attributed to amine salt (N–H) while the one at 1460 cm⁻¹ corresponds to vibrations of –CH₃ bending (Gorgulu and Celik 2013). The band absorption at 1421 cm⁻¹ corresponds to C–O stretching. The band at 1372 cm⁻¹ is related to the vibration of the –CH₂ bending (Gorgulu and Celik 2013) while that at 1320 cm⁻¹ is assigned to C–O groups on the CAS surface. The band at 1154 cm⁻¹ corresponds to antisymmetric bridge C–OR–C stretching (Wang and Shen 2012). The absorption peak at 1033 cm⁻¹ is due to the stretching vibrations of CO, whereas the band at 896 cm⁻¹ is assigned to antisymmetric out-of-ring stretching (Boudechiche et al. 2016). Consequently, the FTIR result indicates that CAS present functional groups that are potential adsorbing and exchanging sites for the interaction with DB86 during biosorption.

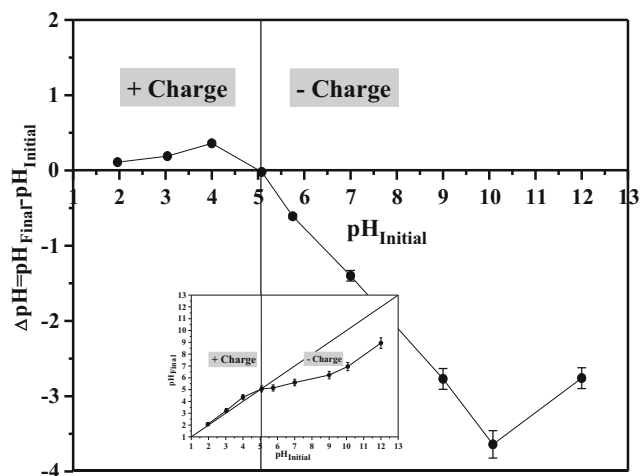


Fig. 2 The determination of the pH_{PZC}

Table 2 Experimental factors and their ranges and standard deviations

Parameters	Units	Factor code	Coded levels and actual values				
			Low axial ($-\alpha = -2$)	Low factorial (-1)	Central (0)	High factorial ($+1$)	High axial ($+\alpha = +2$)
Solution pH	–	X_1	2	3	4	5	6
Biosorbent dose	g L^{-1}	X_2	0.8	1.6	2.4	3.2	4
Initial DB86 concentration	mg L^{-1}	X_3	20	40	60	80	100
Temperature	$^{\circ}\text{C}$	X_4	10	20	30	40	50
$\alpha = (2^k)^{1/4}$	–	–	–	–	–	–	–

Table 3 Central composite rotatable design matrix with experimental and predicted values

Runs	Actual values				Coded values				Response	
	pH	Biosorbent dose	Initial DB86 concentration	T	X_1	X_2	X_3	X_4	Removal experimental (%)	Removal predicted (%)
1	3	1.6	40	20	-1	-1	-1	-1	24.142	24.827
2	5	1.6	40	20	+1	-1	-1	-1	7.614	8.299
3	3	3.2	40	20	-1	+1	-1	-1	43.127	43.812
4	5	3.2	40	20	+1	+1	-1	-1	8.153	8.838
5	3	1.6	80	20	-1	-1	+1	-1	15.105	15.790
6	5	1.6	80	20	+1	-1	+1	-1	3.948	4.633
7	3	3.2	80	20	-1	+1	+1	-1	26.032	26.717
8	5	3.2	80	20	+1	+1	+1	-1	8.338	9.023
9	3	1.6	40	40	-1	-1	-1	+1	27.441	28.126
10	5	1.6	40	40	+1	-1	-1	+1	14.061	14.746
11	3	3.2	40	40	-1	+1	-1	+1	51.942	52.627
12	5	3.2	40	40	+1	+1	-1	+1	33.8	34.485
13	3	1.6	80	40	-1	-1	+1	+1	16.255	16.940
14	5	1.6	80	40	+1	-1	+1	+1	7.983	8.668
15	3	3.2	80	40	-1	+1	+1	+1	32.706	33.391
16	5	3.2	80	40	+1	+1	+1	+1	13.921	14.606
17	2	1.6	60	30	-2	0	0	0	63.653	62.282
18	5	1.6	60	30	+2	0	0	0	13.212	11.841
19	4	0.8	60	30	0	-2	0	0	4.844	3.473
20	4	4	60	30	0	+2	0	0	21.928	20.557
21	4	1.6	20	30	0	0	-2	0	34.783	33.412
22	4	1.6	100	30	0	0	+2	0	7.059	5.688
23	4	1.6	60	10	0	0	0	-2	15.296	13.925
24	4	1.6	60	50	0	0	0	+2	22.96	21.589
25	4	1.6	60	30	0	0	0	0	15.229	15.720
26	4	1.6	60	30	0	0	0	0	15.426	15.720
27	4	1.6	60	30	0	0	0	0	15.9	15.720
28	4	1.6	60	30	0	0	0	0	15.88	15.720
29	4	1.6	60	30	0	0	0	0	15.752	15.720
30	4	1.6	60	30	0	0	0	0	15.95	15.720
31	4	1.6	60	30	0	0	0	0	15.9	15.720

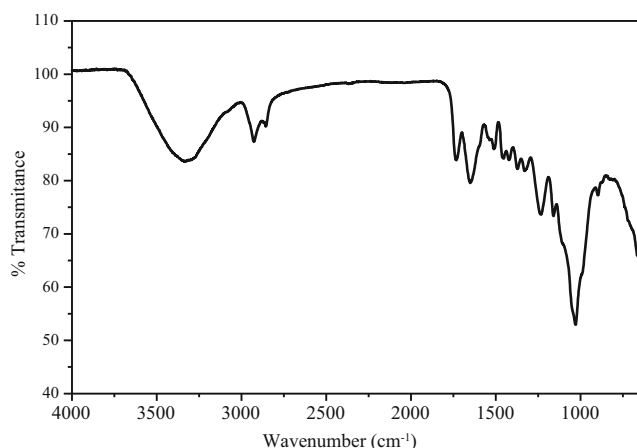


Fig. 3 FTIR spectrum of CAS

SEM/EDS analysis

The SEM morphology of CAS is given in Fig. 4a–d at different magnifications. The surface of CAS exhibits a smooth and non-porous texture; we also note the presence of cavities which are more or less homogeneous with different geometries (Fig. 4c). The EDS spectrum and the content of each

element are given in Fig. 4e. A qualitative chemical composition of CAS was obtained by microanalysis (SEM/EDS); it mainly consists of carbon (69.74%) and oxygen (27.66%), suggesting the existence of the groups C–O, C=O, C–O–C, and O–H and indicating that the predominant functions are of aromatic cycles and alcoholic types: cellulose, lignin, and hemicellulose. Trace elements like Ca, Mg, and P exist between 0.24 and 1.59%.

Experimental design

Main interaction effects and Student's *t* test

The results were analyzed using the JMP release 11.0.0 software, provided by SAS Institute, and the main effects and interactions between the factors were determined. The effect of any factor is defined as the response change produced by a variation of the factor level (Soo et al. 2004). The regression coefficients, associated standard errors, Student's *t* values, and their effects are shown in Tables 3 and 4. By substituting the coefficients in Eq. (2) by their values taken from Tables 3 and 4, one obtains

$$\begin{aligned}
 Y (\%) = & 15.72 - 7.374 X_1 + 7.032 X_2 - 4.856 X_3 + 4.499 X_4 + 5.336 X_1^2 - 0.926 X_2^2 + 0.958 X_3^2 \\
 & + 0.509 X_4^2 - 1.309 X_1^3 - 0.69 X_2^3 - 0.519 X_3^3 - 0.646 X_4^3 - 2.516 X_1 X_2 + 1.695 X_1 X_3 + 1.361 X_1 X_4 - 1.629 X_2 X_3 \\
 & + 1.987 X_2 X_4 - 1.673 X_3 X_4 + 0.385 X_1 X_2 X_3 + 0.607 X_1 X_2 X_4 - 1.137 X_1 X_3 X_4 - 1.103 X_2 X_3 X_4 - 1.104 X_1 X_2 X_3 X_4 \quad (5)
 \end{aligned}$$

This equation includes all terms regardless of their significances. The coefficient sign (\pm) defines the direction of the relationship between the related effect and its response. The positive sign indicates that as the value of one effect changes, the response changes in the same direction, while for the negative sign, the response operates in the opposite direction. The absolute coefficients measure the strength of the relationship (Demim et al. 2013). Table 4 summarizes the regression coefficients accompanied with their standard errors, Student's *t* values, and corresponding *p* values. The *p* and Student's *t* values permit us to know the significance of the model coefficients; the larger the Student's *t* value, the lower the *p* value, and one can obtain a very significant coefficient (Liu and Chiou 2005). The extremely significant effects are X_1^2 (pH²: quadratic effect) followed by X_1 (pH: main factor) and X_3 (initial DB86 concentration) because $|\text{Student's } t \text{ value}| < \text{critical Student's } t \text{ value}$ with probability $p < 0.01\%$ (Wu et al. 2010; Kogkaki et al. 2016). The second effects highly significant ($|\text{Student's } t \text{ value}| < \text{critical Student's } t \text{ value}$ with $p < 1\%$) (Wu et al. 2010; Kogkaki et al. 2016) are X_2 (biosorbent dose), X_4 (temperature), interaction $X_1 X_3$ (pH–initial DB86 concentration), X_1^3 (pH³: cubic effect), and interactions $X_3 X_4$, $X_1 X_2$, $X_2 X_4$, and $X_2 X_3$. The significant third effects

($|\text{Student's } t \text{ value}| < \text{critical Student's } t \text{ value}$ with $p < 5\%$) (Kogkaki et al. 2016) are $X_1 X_4$, X_2^2 (quadratic effect), X_3^2 (quadratic effect), X_3^3 (cubic effect), X_4^3 (cubic effect), $X_1 X_2 X_4$, $X_2 X_3 X_4$, and $X_1 X_2 X_3 X_4$. Based on the Student's *t* test and *p* value ($|\text{Student's } t \text{ value}| > \text{critical Student's } t \text{ value}$ with *p* value $> 5\%$) (Campos et al. 2014), some effects were discarded, because they do not exhibit any statistical significance such as X_2^3 (cubic effect), X_4^2 (quadratic effect), $X_1 X_3 X_4$, and $X_1 X_2 X_3$. Equation (4) is used to visualize the effects of experimental parameters of DB86 removal (Fig. 5). The actual values are determined from the experiments while the predicted ones are obtained from Eq. (5). Both actual and predicted dye removals shown in Fig. 5, the R^2 values ($=0.996$), and the R^2_{adj} ($=0.9827$) indicate a good adjustment between the experimental and predicted responses. The result also suggests that the selected cubic model is adequate for predicting the response variables for the studied parameters.

Analysis of variance

The mathematical cubic models are often unsuitable to describe the experimental data, and a more reliable model is

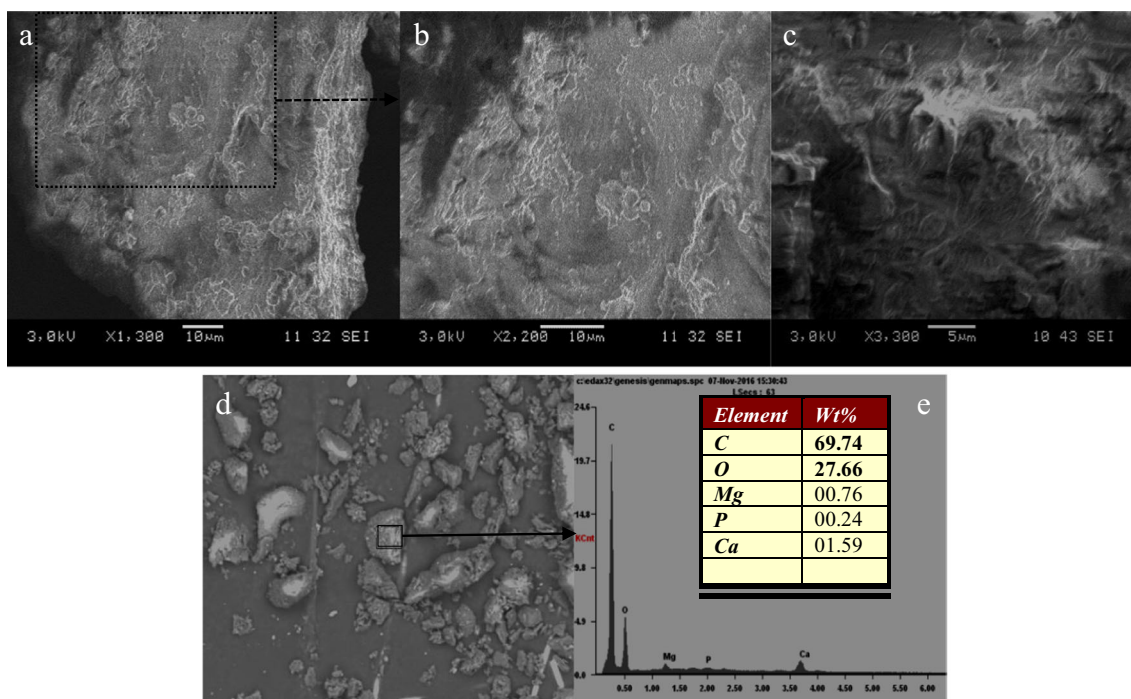


Fig. 4 SEM micrographs of CAS (a–d) and EDS spectrum (e)

required to evaluate the quality of the fitting using ANOVA and to compare the variation sources with the Fisher distribution (Fisher test). This statistical test is based on the ratio of two sums of squares (the error and regression sums of squares). Therefore, the significance of regressions is evaluated by the ratio between the mean square of regression and the mean square of residuals (difference between observed and predicted values) (Almeida et al. 2011).

The ANOVA results for the cubic equation (Table 5) show that the Fisher values for all regressions are higher. A large Fisher value indicates that the cubic model can explain the variation in the DB86 removal. The associated *p* value is used to estimate whether the Fisher value is large enough to indicate statistical significance. *p* values lower than 5% (i.e., $\alpha = 0.05$: error or 95%: confidence) indicate a significant model (Tripathi et al. 2009). The calculated Fisher value 74.86 (which is higher than critical Fisher_{23,7} = 3.42) with very low probability values (*p* value of the model <0.0001) demonstrates that the regression models are significant at 95% of confidence interval for the DB86 removal.

Optimization of independent parameters

RSM combined with CCRD is used to optimize the factors and to describe the nature of the response surface in the experiment using three-dimensional (3D) response surface plots. This combination is helpful for understanding the main factors, and their interactions can provide a simple examination on the effects of independent variables on the removal percentage (Sivarajasekar and Baskar 2014). Therefore, the 3D response surface plots for

the measured removal percentage are based on the cubic polynomial model (Eq. 4). Figure 6a–f presents the 3D response surface plots as a function of two simultaneous parameters, maintaining the other parameters at a fixed central level ($X = 0$). As observed, these plots display reasonable interactions between each of the independent factors and the DB86 removal percentage. Figure 6a gives the response surface plots of pH and biosorbent dose. The DB86 removal increases drastically from 3 to 77% with decreasing pH from 6 to 2 and increasing the biosorbent dose from 0.8 to 4 g L⁻¹. This can be explained by the fact that in an acidic medium, DB86 is dissociated to polar groups (R–SO₃⁻). Moreover, low pH is favorable for the biosorption of anionic DB86 on CAS because the biosorbent is acidic and increases the H⁺ concentration on its surface. In addition, the CAS amount is very significant (biosorbent dose = 4 g L⁻¹), which induces electrostatic interactions between its surface and R–SO₃⁻ from the solution (Cheng et al. 2015). At a low pH (< p*H*_{PZC} = 5.06), the exchange sites on the biosorbent are positive, thus favoring the biosorption of anions (R–SO₃⁻) (Cheng et al. 2015). According to Mahmoodi et al. (2011) who have used direct red 23 and acid green 25 as anionic dyes at pH 2, strong Coulomb attractions exist between the positively charged surfaces of the biosorbent (due to the ionization of functional groups of biosorbent) and the negatively charged anionic dyes. Aksu and Isoglu (2006) studied the pH’s effect on the removal of Gemazol turquoise blue G, as an anionic reactive dye, on sugar beet pulp; they noticed that the adsorption peaks at pH 2 with an adsorption capacity of 83.7 mg g⁻¹ and decreases with further pH increase to reach zero at pH 6. Figure 6b presents the response surface plots in the pH range 2–6 and initial DB86 concentration

Table 4 Statistical analysis of coefficients from the cubic model

Coefficient	Estimate parameter	Standard error	Student t-value	Significant or not significant factors critical student t-test= 2.365	p-value
Constant	a ₀	15.71957	0.685488	22.93	<0.0001***
X ₁ *X ₁	a ₁₁	5.335503	0.339155	15.73	<0.0001***
X ₁	a ₁	-7.374250	0.641215	-11.5	<0.0001***
X ₃	a ₃	7.032167	0.641215	10.97	<0.0001***
X ₂	a ₂	-4.855667	0.641215	-7.57	0.0001**
X ₄	a ₄	4.498833	0.641215	7.02	0.0002**
X ₁ *X ₃	a ₁₃	-2.516125	0.453408	-5.55	0.0009**
X ₁ *X ₁ *X ₁	a ₁₁₁	-1.309000	0.261775	-5	0.0016**
X ₃ *X ₄	a ₃₄	1.986750	0.453408	4.38	0.0032**
X ₁ *X ₂	a ₁₂	1.694750	0.453408	3.74	0.0073**
X ₂ *X ₄	a ₂₄	-1.672875	0.453408	-3.69	0.0078**
X ₂ *X ₃	a ₂₃	-1.628625	0.453408	-3.59	0.0088**
X ₁ *X ₄	a ₁₄	1.360875	0.453408	3	0.0199*
X ₂ *X ₂	a ₂₂	0.957628	0.339155	2.82	0.0256*
X ₃ *X ₃	a ₃₃	-0.926122	0.339155	-2.73	0.0293*
X ₃ *X ₃ *X ₃	a ₃₃₃	-0.690292	0.261775	-2.64	0.0336*
X ₁ *X ₂ *X ₄	a ₁₂₄	-1.136625	0.453408	-2.51	0.0406*
X ₄ *X ₄ *X ₄	a ₄₄₄	-0.645708	0.261775	-2.47	0.0430*
X ₁ *X ₂ *X ₃ *X ₄	a ₁₂₃₄	-1.103750	0.453408	-2.43	0.0451*
X ₂ *X ₃ *X ₄	a ₂₃₄	-1.102750	0.453408	-2.43	0.0453*
X ₂ *X ₂ *X ₂	a ₂₂₂	-0.518833	0.261775	-1.98	0.0879
X ₄ *X ₄	a ₄₄	0.509378	0.339155	1.5	0.1768
X ₁ *X ₃ *X ₄	a ₁₃₄	0.606750	0.453408	1.34	0.2227
X ₁ *X ₂ *X ₃	a ₁₂₃	0.384875	0.453408	0.85	0.4240

p, probability

*** Extremely significant ; ** Highly significant; * significant

from 20 to 100 mg L⁻¹; the biosorbent dose and temperature are maintained at a fixed central level, 2.4 g L⁻¹ and 30 °C, respectively. The results showed that DB86 removal percentage remarkably increases with decreasing pH to reach 87% at pH 2 at low initial DB86 concentration (=20 mg L⁻¹). This phenomenon can be attributed to the acidic medium favorable for the biosorption, at low DB86 concentration and high biosorbent dose (2.4 g L⁻¹). However, for higher DB86 concentrations, the removal percentage decreases because of the saturation of CAS sites on the surface (Sivarajasekar and Baskar 2014; Abbasi and Habibi 2016). The surface plot (Fig. 6c) indicates the evolution of DB86 removal by varying the pH simultaneously from 2 to 6 and the temperature from 10 to 50 °C, maintaining

the other factors at their fixed central levels (initial DB86 concentration = 60 mg L⁻¹ and biosorbent dose = 2.4 g L⁻¹). From this response surface plot, we note a maximum DB86 removal of 66% at pH 2 and 10 °C; similar results were reported elsewhere (Arunachalam and Annadurai 2011). Figure 6d illustrates the surface plot of the variation of DB86 removal for the biosorbent dose (0.8–4 g L⁻¹) and initial DB86 concentration (20 to 100 mg L⁻¹) with appropriate values of other parameters at center levels (pH 4 and temperature 30 °C). From this response surface plot, a maximum DB86 removal of 45% was obtained for an initial DB86 concentration of 20 mg L⁻¹ and a biosorbent dose of 4 g L⁻¹. The low removal is attributed to pH (=4) which plays a crucial role in the biosorption. Similar results were

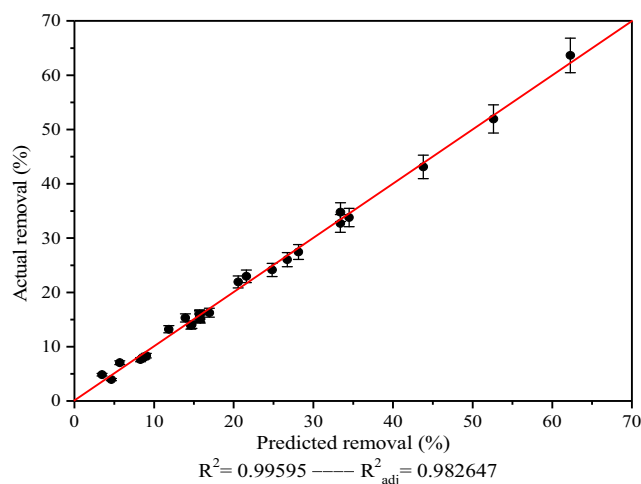


Fig. 5 Actual and predicted values for DB86 removal

reported by Cheng et al. (2015) who have studied the congo red and direct red 80 adsorptions onto activated carbon–surfactant from aqueous solutions by using the RSM–Box–Behneken design where the optimal values are 20 mg L⁻¹ and 50 °C. It can be concluded that these results indicate the optimum conditions for DB86 removal on CAS (theoretical maximum removal) using CCRD by a cubic model (minimum level of X₁, X₃, X₄ = -α, and maximum level of X₂ = +α). Theoretical DB86 removal of 123% was found under optimum conditions: pH 2, biosorbent dose of 4 g L⁻¹, initial DB86 concentration of 20 mg L⁻¹, and temperature of 10 °C (Fig. 6e, f). The experience was performed from these optimized parameters, and the result shows that DB86 removal was 100%.

Biosorption isotherm

The Langmuir, Freundlich, and Temkin models have been applied to determine the nature of DB86 biosorption isotherms on CAS. The Langmuir model based on a biosorption monolayer on the biosorbent surface, with no interaction between adsorbed molecules (Hosseini et al. 2011), is expressed by

$$q_e = \frac{q_{max}K_L C_e}{(1 + K_L C_e)} \tag{6}$$

The linearized form is represented by

$$\frac{C_e}{q_e} = \frac{1}{q_{max}K_L} + \frac{C_e}{q_{max}} \tag{7}$$

where q_{max} and K_L are, respectively, the maximum biosorption capacity to form a complete monolayer on the surface (mg g⁻¹) and the Langmuir constant related to the biosorption energy (L mg⁻¹).

The empirical Freundlich model describes the biosorption on heterogeneous surface through a multilayer biosorption mechanism (Hosseini et al. 2011):

$$q_e = K_F C_e^{1/n} \tag{8}$$

The linearized form is expressed by Eq. (9)

$$\ln q_e = \ln K_F + \frac{1}{n} \ln C_e \tag{9}$$

where K_F [(mg g⁻¹) (L mg⁻¹)^{1/n}] is the Freundlich constant and 1/n is the heterogeneity factor, related to the capacity and biosorption intensity.

The Temkin isotherm contains a parameter, which does not neglect the adsorbate–biosorbent interactions and supposes that (i) the biosorption heat of DB86 molecules in the layer decreases linearly with increasing the coverage and (ii) the biosorption is characterized by a homogeneous distribution of binding energies (Ghaedi et al. 2014).

$$q_e = \left(\frac{RT}{b_T}\right) \ln(A_T C_e) \tag{10}$$

The linear form of Eq. (10) gives

$$q_e = \frac{RT}{b_T} \ln(A_T) + \frac{RT}{b_T} \ln(C_e) \tag{11}$$

where b_T (J mol⁻¹) is the Temkin constant related to the biosorption heat of DB86 and A_T (L mg⁻¹) the equilibrium binding constant.

The equilibrium data were obtained at different concentrations (20–100 mg L⁻¹) during 180 min of fixed contact time at constant pH (=2), a biosorbent dosage of 2 g L⁻¹, and a temperature of 20 °C. The parameters of all isotherm models are gathered in Table 6. Accordingly, the R² value for the Langmuir model (close to 1) is greater than that of Freundlich and Temkin models (Table 6 and Fig. 7a–c) and this indicates that the homogeneous biosorption sites are occupied by one layer of DB86 molecules (Noorimotlagh et al. 2014) with a maximum biosorption capacity (q_{max}) of 24.02 mg g⁻¹ (Table 6 and Fig. 7a). The graphical analysis (Fig. 7d)

Table 5 ANOVA for response surface cubic model

Source	Degree of freedom	Sum of squares	Mean square	Fisher value	p value
Regression	23	5663.432	246.236	74.861	<0.0001
Residual	7	23.025	3.289		
Total	30	5686.457			

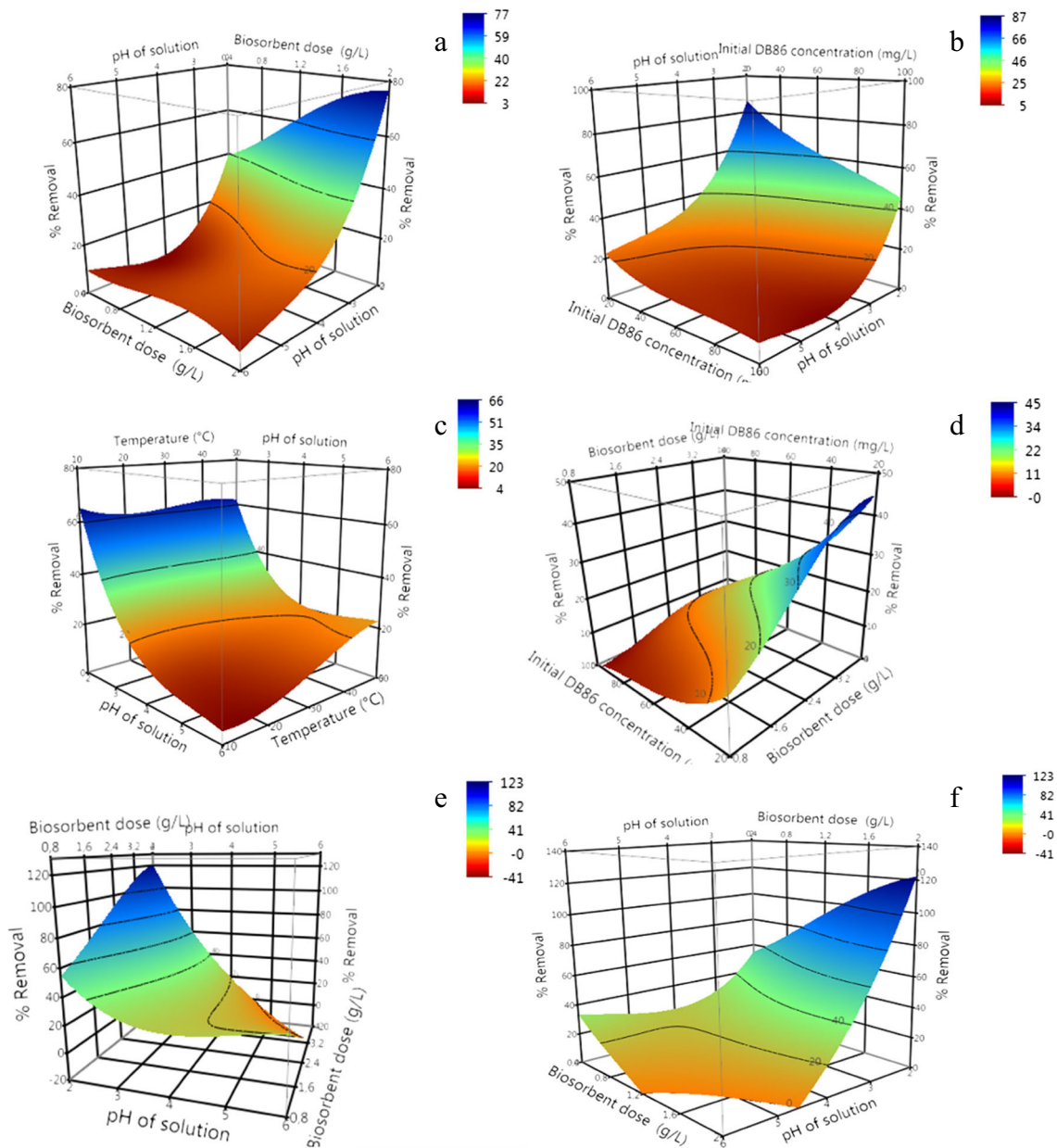


Fig. 6 Response surface plots (3D) of DB86 removal versus the effects (pH of solution, biosorbent dose, initial DB86 concentration, and temperature)

confirms the best fit of the experimental data by the Langmuir model. Saygılı and Güzel (2016) explored the adsorption isotherm of yellow anionic acid on a low-cost activated carbon using ZnCl_2 for chemical activation. The equilibrium data are well-fitted by the Langmuir model ($R^2 = 0.997$) compared to the Freundlich one. El Nemr et al. (2009) confirmed the successful application of the Langmuir model to the experimental data for DB86 adsorption on activated carbon prepared from orange peel. The Langmuir isotherm fits suitably the experimental data with the q_{\max} value close to those obtained with other adsorbents using anionic dyes. It is clear that CAS used in this work have an acceptable

maximum biosorption capacity of the Langmuir model compared to other adsorbents reported in the literature (Table 7).

Biosorption kinetics

The kinetic study of DB86 biosorption on CAS was undertaken for different initial DB86 concentrations; it provides information for biosorption modeling and predicts the biosorption rate. For this purpose, the pseudo-first-order, pseudo-second-order, and intraparticle diffusion models were used.

Table 6 Constants of isotherm models for the biosorption of DB86

Langmuir isotherm			Freundlich isotherm			Temkin isotherm		
q_{\max} (mg g ⁻¹)	K_L (L g ⁻¹)	R^2	K_F ((mg g ⁻¹)(L mg ⁻¹) ^{1/n})	n	R^2	A_T (L mg ⁻¹)	b_T (J mol ⁻¹)	R^2
24.02	1.138	0.99	12.75	5.61	0.90	109.28	850.69	0.94

The Lagergren first-order model is given by

$$\log(q_e - q_t) = \log q_e - \frac{k_1 t}{2.303} \tag{12}$$

where q_t and q_e are the biosorption capacities, respectively, at time t and at equilibrium (mg g⁻¹) and k_1 (min⁻¹) is the biosorption rate constant.

The pseudo-second order model is expressed by

$$\frac{t}{q_t} = \frac{1}{k_2 q_e^2} + \frac{1}{q_e} t \tag{13}$$

where k_2 (g mg⁻¹ min⁻¹) is the pseudo-second-order rate constant. The initial biosorption rate h (mg g⁻¹ min⁻¹) is given by (Arunachalam and Annadurai 2011)

$$h = k_2 q_e^2 \tag{14}$$

Figure 8a, b presents the plots for the pseudo-first-order and pseudo-second-order kinetic models, respectively, and the model constants are gathered in Table 8. The biosorption kinetic of DB86 follows a pseudo-second-order model in the concentration range 20–100 mg L⁻¹ with very high correlation coefficients $R^2 > 0.99$, and the calculated equilibrium biosorption capacities ($q_{e \text{ cal}}$) are much closer to the experimental ones ($q_{e \text{ exp}}$). By contrast, the pseudo-first-order model does not give a good agreement with the experimental data ($R^2 = 0.504\text{--}0.947$), and the experimental biosorption capacities are different from the calculated ones (Table 8). Sadaf and Bhatti (2011) reported similar results for the removal of

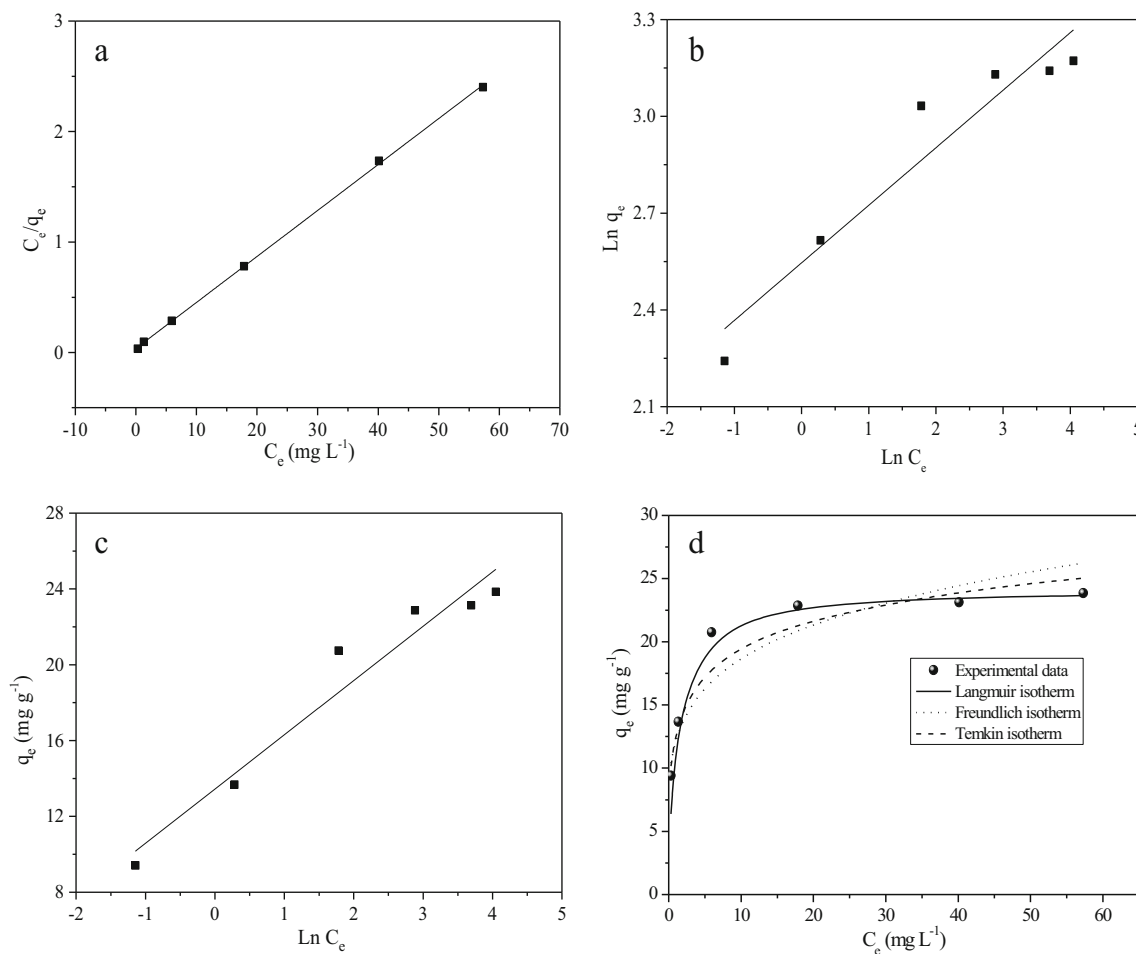


Fig. 7 The biosorption isotherm plots: **a** Langmuir, **b** Freundlich, **c** Temkin, and **d** graphical analyses

Table 7 Comparison of the q_{\max} of various adsorbents used for anionic dye removal from aqueous solutions

Adsorbents	Anionic dyes	pH	q_{\max} (mg g ⁻¹)	Reference
<i>Crataegus azarolus</i> stones	Direct blue 86	2	24.02	Present work
Olive stone	Alizarin red S	3.28	16.10	Albadarin and Mangwandi (2015)
Almond shell	Acid blue 129	2	11.95	Fat'hi et al. (2014)
<i>Sargassum glaucescens</i>	Acid black 1	2	27.2	Daneshvar et al. (2012)
<i>Stoechospermum marginatum</i>	Acid black 1	2	29.6	Daneshvar et al. (2012)
Rice husk	Direct orange 26	3	19.96	Safa and Bhatti (2011)
Cashew nut shell	Congo red	2	5.18	Kumar et al. (2010)
Orange peel-activated carbon	Direct blue 86	2	33.78	El Nemr et al. (2009)
Mixture of almond shells	Direct red 80	2	22.42	Ardejani et al. (2008)
Orange peel	Direct blue 80	2	21.05	Arami et al. (2005)

anionic dye Foron turquoise SBLN by using fungal biomass as biosorbent. The pseudo-second-order rate constant (k_2) decreases with increasing the DB86 concentration (Table 8), and this can be attributed to the competitive biosorption of DB86 molecules on available surface area (Albadarin et al. 2011).

The Weber–Morris equation is used to describe the intraparticle diffusion. If the plot of q_t versus $t^{1/2}$ is linear and passes by the origin, then the intraparticle diffusion is the sole rate-limiting step (Albadarin et al. 2011) and the rate constant (k_{int} , mg g⁻¹ min^{-1/2}) is given by the equation (Abbas and Trari 2015)

$$q_t = k_{\text{int}}t^{1/2} + C \quad (15)$$

where C (mg g⁻¹) is the intercept due to the presence of the boundary layer thickness (Albadarin et al. 2011; Boudechiche et al. 2016). A non-zero value for the intercept indicates that a mass transfer limits the diffusion rate across the boundary

layer (Albadarin et al. 2011). The plots q_t versus $t^{1/2}$ (Fig. 9) are multilinear ($R^2 = 0.92–0.98$), and the straight lines do not pass by the origin (boundary layer effect) (Table 8). This characterizes some degree of boundary layer control, which clearly indicates that the intraparticle diffusion is not the rate-determining step. So, other kinetic models control the biosorption of DB86 on CAS which can operate simultaneously (Albadarin et al. 2011).

Conclusion

In the present work, RSM combined with CCRD was used to examine the effects of four operating parameters, namely, the initial solution pH (X_1), biosorbent dose (X_2), initial DB86 concentration (X_3), and temperature (X_4), for DB86 removal by a novel biosorbent: *C. azarolus*. The cubic model was

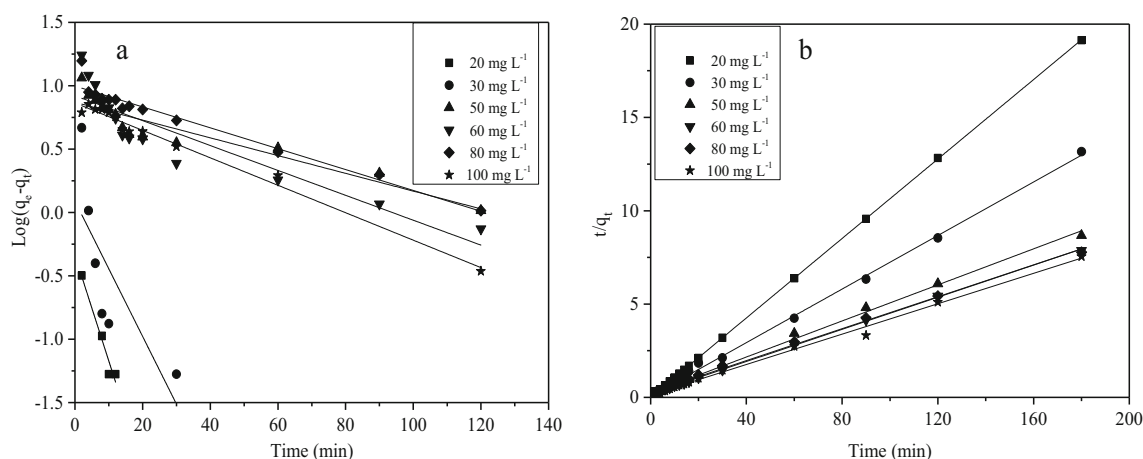
**Fig. 8** The kinetic plots, pseudo-first-order (a) and pseudo-second-order (b) models

Table 8 Kinetic parameters for the DB86 biosorption

C_0 (mg L ⁻¹)	$q_{e,exp.}$ (mg g ⁻¹)	Pseudo-first order			Pseudo-second order				Intraparticle diffusion		
		$q_{e,cal}$ (mg g ⁻¹)	k_1 (min ⁻¹)	R^2	$q_{e,cal}$ (mg g ⁻¹)	h (mg g ⁻¹ min ⁻¹)	k_2 (g mg ⁻¹ min ⁻¹)	R^2	k_{int} (mg g ⁻¹ min ^{-1/2})	C (mg g ⁻¹)	R^2
20	9.408	0.458	0.192	0.9418	9.4384	467.289	5.245	1	–	–	–
30	13.675	1.227	0.123	0.5038	13.937	16.059	8.267×10^{-2}	0.9984	1.067	11.087	0.9151
50	20.751	7.398	0.016	0.8568	20.7	4.359	1.017×10^{-2}	0.997	1.697	8.987	0.9766
60	22.871	8.339	0.023	0.8054	23.229	4.99	9.247×10^{-3}	0.9995	3.214	6.326	0.9447
80	23.136	9.944	0.019	0.947	23.381	3.87	7.08×10^{-3}	0.9976	1.004	12.248	0.9835
100	23.852	7.316	0.025	0.985	24.570	7.542	1.249×10^{-2}	0.9948	1.177	14.412	0.9811

found to be a suitable mathematical model which provides an adequate prediction of DB86 removal ($R^2 = 0.996$ and $R^2_{adj} = 0.983$). According to this model, the Student's t test results showed that all coefficients are significant except X_2^3 , X_4^2 , $X_1 * X_3 * X_4$, and $X_1 * X_2 * X_3$. Additionally, the optimal conditions resulting in the highest DB86 removal of theoretical and experimental values, 123 and 100%, respectively, were obtained for a solution of pH 2, a biosorbent dose of 4 g L⁻¹, an initial DB86 concentration of 20 mg L⁻¹, and a temperature of 10 °C. The equilibrium data of DB86 biosorption onto CAS are well-fitted by the Langmuir model with a maximum monolayer biosorption capacity of 24.02 mg g⁻¹. The kinetic study showed that the pseudo-second-order model describes adequately the DB86 biosorption, and the intraparticle diffusion model is not the rate-limiting step which governs the biosorption mechanism; other kinetic models may control the biosorption rate.

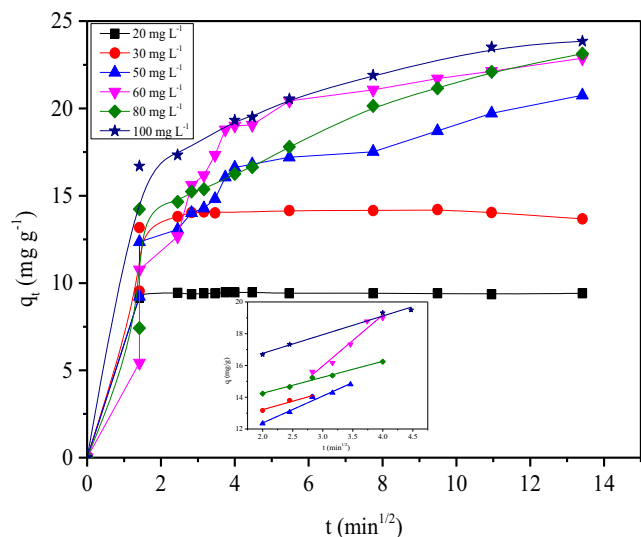


Fig. 9 The intraparticle diffusion model at various initial DB86 concentrations

References

Abbas M, Trari M (2015) Kinetic, equilibrium and thermodynamic study on the removal of congo red from aqueous solutions by adsorption onto apricot stone. *Process Saf Environ Prot* 98:424–436

Abbasi M, Habibi MM (2016) Optimization and characterization of direct blue 71 removal using nanocomposite of chitosan-MWCNTs: central composite design modeling. *J Taiwan Inst Chem Eng* 62:112–121

Afshar S, Sadehvand M, Azad A, Dekamin MG, Jalali-Heravi M, Mollahosseini A, Amani M, Tadjarodi A (2015) Optimization of catalytic activity of sulfated titania for efficient synthesis of isoamyl acetate by response surface methodology. *Monatsh Chemie Chem Mon* 146:1949–1957

Ahmadi S, Manteghian M, Kazemian H, Rohani S, Darian JT (2012) Synthesis of silver nano catalyst by gel-casting using response surface methodology. *Powder Technol* 228:163–170

Akar ST, Sayin F, Turkyilmaz S, Akar T (2014) Multivariate optimization of the decolorization process by surface modified biomaterial: Box–Behnken design and mechanism analysis. *Environ Sci Pollut Res* 21:3055–13068

Aksu Z, Isoglu A (2006) Use of agricultural waste sugar beet pulp for the removal of Gemazol turquoise blue-G reactive dye from aqueous solution. *J Hazard Mater* 137:418–430

Albadarin AB, Mangwandi C (2015) Mechanisms of alizarin red S and methylene blue biosorption onto olive stone by-product: isotherm study in single and binary systems. *J Environ Manag* 164:86–93

Albadarin AB, Al-Muhtase AH, Walker GM, Allen SJ, Ahmad MNM (2011) Retention of toxic chromium from aqueous phase by H₃PO₄-activated lignin: effect of salts and desorption studies. *Desalination* 274:64–73

Almeida LC, Garcia-Segura S, Bocchi N, Brillas E (2011) Solar photoelectro-Fenton degradation of paracetamol using a flow plant with a Pt/air-diffusion cell coupled with a compound parabolic collector: process optimization by response surface methodology. *Appl Catal B Environ* 103:21–30

Arami M, Limaee NY, Mahmoodi NM, Tabrizi NS (2005) Removal of dyes from colored textile wastewater by orange peel adsorbent: equilibrium and kinetic studies. *J Colloid Interface Sci* 288:371–376

Ardejani FD, Badii K, Limaee NY, Shafaei SZ, Mirhabibi AR (2008) Adsorption of direct red 80 dye from aqueous solution onto almond shells: effect of pH, initial concentration and shell type. *J Hazard Mater* 151:730–737

Arunachalam R, Annadurai G (2011) Optimized response surface methodology for adsorption of dyestuff from aqueous solution. *J Environ Sci Technol* 4:65–72

- Asfaram A, Ghaedi M, Ghezalbash GR, Dil EA, Tyagi I, Agarwal S, Gupta VK (2016) Biosorption of malachite green by novel biosorbent *Yarrowia lipolytica* isf7: application of response surface methodology. *J Mol Liq* 214:249–258
- Aytar P, Gedikli S, Sam M, Farizoğlu B, Çabuk A (2013) Sequential treatment of olive oil mill wastewater with adsorption and biological and photo-Fenton oxidation. *Environ Sci Pollut Res* 20:3060–3067
- Bazrafshan Z, Ataefard M, Nourmohammadian F (2015) Modeling the effect of pigments and processing parameters in polymeric composite for printing ink application using the response surface methodology. *Prog Org Coat* 82:68–73
- Boudechiche N, Mokaddem H, Sadaoui Z, Trari M (2016) Biosorption of cationic dye from aqueous solutions onto lignocellulosic biomass (*Luffa cylindrica*): characterization, equilibrium, kinetic and thermodynamic studies. *Int J Ind Chem* 7:167–180
- Campos MI, Figueiredo TVB, Sousa LS, Druzian JI (2014) The influence of crude glycerin and nitrogen concentrations on the production of PHA by *Cupriavidus necator* using a response surface methodology and its characterizations. *Ind Crop Prod* 52:338–346
- Cheng Z, Zhang L, Guo X, Jiang X, Li T (2015) Adsorption behavior of direct red 80 and congo red onto activated carbon/surfactant: process optimization, kinetics and equilibrium. *Spectrochim Acta A Mol Biomol Spectrosc* 137:1126–1143
- Daneshvar E, Kousha M, Jokar M, Koutahzadeh N, Guibal E (2012) Acidic dye biosorption onto marine brown macroalgae: isotherms, kinetic and thermodynamic studies. *Chem Eng J* 204–206:225–234
- Demim S, Drouiche N, Aouabed A, Semsari S (2013) CCD study on the ecophysiological effects of heavy metals on *Lemna gibba*. *Ecol Eng* 57:302–313
- El Khames SM, Khiari R, Elaloui E, Moussaoui Y (2014) Adsorption of anthracene using activated carbon and *Posidonia oceanica*. *Arab J Chem* 7:109–113
- El Messaoudi N, El Khomri M, Dbik A, Bentahar S, Lacherai A, Bakiz B (2016) Biosorption of congo red in a fixed-bed column from aqueous solution using jujube shell: experimental and mathematical modeling. *J Environ Chem Eng* 4:3848–3855
- El Nemr A, Abdelwahab O, El-Sikaily A, Khaled A (2009) Removal of direct blue-86 from aqueous solution by new activated carbon developed from orange peel. *J Hazard Mater* 161:102–110
- El-Ashtoukhy ESZ, Fouad YO (2015) Liquid–liquid extraction of methylene blue dye from aqueous solutions using sodium dodecylbenzene sulfonate as an extractant. *Alex Eng J* 54:77–81
- Fat'hi MR, Asfaram A, Hadipour A, Roosta M (2014) Kinetics and thermodynamic studies for removal of acid blue 129 from aqueous solution by almond shell. *J Environ Health Sci Eng* 12:62
- Ferkous H, Hamdaoui O, Merouani S (2015) Sonochemical degradation of naphthol blue black in water: effect of operating parameters. *Ultrason Sonochem* 26:40–47
- Ghaedi M, Zeinali N, Ghaedi AM, Teimuori M, Tashkhourian J (2014) Artificial neural network-genetic algorithm based optimization for the adsorption of methylene blue and brilliant green from aqueous solution by graphite oxide nanoparticle. *Spectrochim Acta A Mol Biomol Spectrosc* 125:264–277
- Gorgulu AA, Celik S (2013) Biosorption potential of orange G dye by modified *Pyracantha coccinea*: batch and dynamic flow system applications. *Chem Eng J* 226:263–270
- Gupta VK, Eren T, Atar N, Yola ML, Parlak C, Karimi-Maleh H (2015) $\text{CoFe}_2\text{O}_4/\text{TiO}_2$ decorated reduced graphene oxide nanocomposite for photocatalytic degradation of chlorpyrifos. *J Mol Liq* 208:122–129
- Gupta VK, Agarwal S, Olgun A, Demir Hİ, Yola ML, Atar N (2016) Adsorptive properties of molasses modified boron enrichment waste based nanoclay for removal of basic dyes. *J Ind Eng Chem* 34:244–249
- Hosseini S, Khan MA, Malekbala MR, Cheah W, Choong TSY (2011) Carbon coated monolith, a mesoporous material for the removal of methyl orange from aqueous phase: adsorption and desorption studies. *Chem Eng J* 171:1124–1131
- Jain M, Garg VK, Kadirvelu K (2011) Investigation of Cr(VI) adsorption onto chemically treated *Helianthus annuus*: optimization using response surface methodology. *Bioresour Technol* 102:600–605
- Kebir M, Trari M, Maachi R, Nasrallah N, Amrane A (2015) Valorization of *Inula viscosa* waste extraction, modeling of isotherm, and kinetic for the tartrazine dye adsorption. *Desalin Water Treat* 54:2806–2816
- Kesraoui A, Moussa A, Ben G, Ben Ali G, Seffen M (2016) Biosorption of alpacide blue from aqueous solution by lignocellulosic biomass: *Luffa cylindrica* fibers. *Environ Sci Pollut Res* 23:15832–15840
- Khiari S, Boussaid M, Messaoud C (2014) Genetic diversity and population structure in natural populations of Tunisian Azarole (*Crataegus azarolus* L. var. *aronia* L.) assessed by microsatellite markers. *Biochem Syst Ecol* 58:264–270
- Kogkaki EA, Natskoulis PI, Panagou EZ (2016) Modeling the effect of natamycin, pine-resin and environmental factors on the growth and OTA production by *Aspergillus carbonarius* using response surface methodology. *Food Res Int* 79:19–28
- Kousha M, Tavakoli S, Daneshvar E, Vazirzadeh A, Bhatnagar A (2015) Central composite design optimization of acid blue 25 dye biosorption using shrimp shell biomass. *J Mol Liq* 207:266–273
- Kumar PS, Ramalingam S, Senthamarai C, Niranjana M, Vijayalakshmi P, Sivanesan S (2010) Adsorption of dye from aqueous solution by cashew nut shell: studies on equilibrium isotherm, kinetics and thermodynamics of interactions. *Desalination* 261:52–60
- Kuppusamy S, Thavamani P, Megharaj M, Venkateswarlu K, Lee YB, Naidu R (2016) Potential of *Melaleuca diosmifolia* as a novel, non-conventional and low-cost coagulating adsorbent for removing both cationic and anionic dyes. *J Ind Eng Chem* 37:198–207
- Li M, Wu SC, Peng YH, Shih Y (2016) Adsorption of volatile organic vapors by activated carbon derived from rice husk under various humidity conditions and its statistical evaluation by linear solvation energy relationships. *Sep Purif Technol* 170:102–108
- Liu HL, Chiou YR (2005) Optimal decolorization efficiency of reactive red 239 by UV/TiO₂ photocatalytic process coupled with response surface methodology. *Chem Eng J* 112:173–179
- de Luna MDG, Flores ED, Genuino DAD, Futral CM, Wan M-W (2013) Adsorption of Eriochrome black T (EBT) dye using activated carbon prepared from waste rice hulls—optimization, isotherm and kinetic studies. *J Taiwan Inst Chem Eng* 44:646–653
- Mahmoodi NM, Salehi R, Arami M, Bahrami H (2011) Dye removal from colored textile wastewater using chitosan in binary systems. *Desalination* 267:64–72
- Mazaheri H, Ghaedi M, Hajati S, Dashtian K, Purkait MK (2015) Simultaneous removal of methylene blue and Pb^{2+} ions using ruthenium nanoparticle-loaded activated carbon: response surface methodology. *RSC Adv* 5:83427–83435
- Mook WT, Ajeel MA, Aroua MK, Szlachta M (2017) The application of iron mesh double layer as anode for the electrochemical treatment of reactive black 5 dye. *J Environ Sci* 54:184–195
- Mozia S, Janus M, Brożek P, Bering S, Tamowski K, Mazur J, Morawski AW (2016) A system coupling hybrid biological method with UV/O₃ oxidation and membrane separation for treatment and reuse of industrial laundry wastewater. *Environ Sci Pollut Res* 23:19145–19155
- Noorimotlagh Z, Soltani RDC, Khataee AR, Nourmoradi SSH (2014) Adsorption of a textile dye in aqueous phase using mesoporous activated carbon prepared from Iranian milk vetch. *J Taiwan Inst Chem Eng* 45:1783–1791
- Oladipo AA, Gazi M, Saber-Samandari S (2014) Adsorption of anthraquinone dye onto eco-friendly semi-IPN biocomposite hydrogel: equilibrium isotherms, kinetic studies and optimization. *J Taiwan Inst Chem Eng* 45:653–664
- Pathak PD, Mandavgane SA (2015) Preparation and characterization of raw and carbon from banana peel by microwave activation: application in citric acid adsorption. *J Environ Chem Eng* 3:2435–2447

- Podstawczyk D, Witek-Krowiaka A, Dawieca A, Bhatnagar A (2015) Biosorption of copper(II) ions by flax meal: empirical modeling and process optimization by response surface methodology (RSM) and artificial neural network (ANN) simulation. *Ecol Eng* 83:364–379
- Sadaf S, Bhatti HN (2011) Biosorption of Foron turquoise SBLN using mixed biomass of white rot fungi from synthetic effluents. *Afr J Biotechnol* 10(62):13548–13554
- Safa Y, Bhatti HN (2011) Kinetic and thermodynamic modeling for the removal of direct red-31 and direct Orange-26 dyes from aqueous solutions by rice husk. *Desalination* 272:313–322
- Salehi I, Shirani M, Semnani A, Hassani M, Habibollahi S (2016) Comparative study between response surface methodology and artificial neural network for adsorption of crystal violet on magnetic activated carbon. *Arab J Sci Eng* 41:2611–2621
- Saygılı H, Güzel F (2016) High surface area mesoporous activated carbon from tomato processing solid waste by zinc chloride activation: process optimization, characterization and dyes adsorption. *J Clean Prod* 113:995–1004
- Silva MMF, Oliveira MM, Avelino MC, Fonseca MG, Almeida RKS, Silva Filho EC (2012) Adsorption of an industrial anionic dye by modified-KSF-montmorillonite: evaluation of the kinetic, thermodynamic and equilibrium data. *Chem Eng J* 203:259–268
- Šimek M, Mikulášek P, Kalenda P, Weidlich T (2016) Possibilities for removal of chlorinated dye mordant blue 9 from model waste water. *Chem Pap* 70:470–476
- Sivarajasekar N, Baskar R (2014) Adsorption of basic red 9 on activated waste *Gossypium hirsutum* seeds: process modeling, analysis and optimization using statistical design. *J Ind Eng Chem* 20:2699–2709
- Soo EL, Salleh AB, Basri M, Rahman RNZA, Kamaruddin K (2004) Response surface methodological study on lipase-catalyzed synthesis of amino acid surfactants. *Process Biochem* 39:1511–1518
- Sun S, Yang J, Li Y, Wang K, Li X (2014) Optimizing adsorption of Pb(II) by modified litchi pericarp using the response surface methodology. *Ecotoxicol Environ Saf* 108:29–35
- Tripathi P, Srivastava VC, Kumar A (2009) Optimization of an azo dye batch adsorption parameters using Box–Behnken design. *Desalination* 249:1273–1279
- Varala S, Dharanija B, Satyavathi B, Basava Rao VV, Parthasarathy R (2016) New biosorbent based on deoiled karanja seed cake in biosorption studies of Zr(IV): optimization using Box–Behnken method in response surface methodology with desirability approach. *Chem Eng J* 302:786–800
- Verma AK, Dash RR, Bhunia P (2012) A review on chemical coagulation/flocculation technologies for removal of colour from textile wastewaters. *J Environ Manag* 93:154–168
- Vijayaraghavan K, Won SW, Mao J, Yun YS (2008) Chemical modification of *Corynebacterium glutamicum* to improve methylene blue biosorption. *Chem Eng J* 145:1–6
- Wang Y, Shen XY (2012) Optimum plasma surface treatment of Luffa fibers. *J Macromol Sci Part B Phys* 51:662–670
- Wu H, Feng TC, Chung TW (2010) Studies of VOCs removed from packed-bed absorber by experimental design methodology and analysis of variance. *Chem Eng J* 157:1–17
- Xie M, Dunford NT, Goad C (2011) Enzymatic extraction of wheat germ oil. *J Am Oil Chem Soc* 88:2015–2021
- Yola ML, Eren T, Atar N (2014a) A novel efficient photocatalyst based on TiO₂ nanoparticles involved boron enrichment waste for photocatalytic degradation of atrazine. *Chem Eng J* 250:288–294
- Yola ML, Eren T, Atar N, Wang S (2014b) Adsorptive and photocatalytic removal of reactive dyes by silver nanoparticle-colemanite ore waste. *Chem Eng J* 242:333–340